Vol. 39, No. 2 (2017) 152-167, DOI: 10.24874/ti.2017.39.02.02

Tribology in Industry

www.tribology.fink.rs

RESEARCH

Dynamic Simulation of a Mobile Manipulator with Joint Friction

V. Chacko[a], Z.A. Khan [a]

[a]*NanoCorr, Energy & Modelling (NCEM) Research Group, Department of Design and Engineering, Faculty of Science & Technology, Bournemouth University, United Kingdom BH12 5BB.*

Keywords:

Virtual prototyping
Manipulator
Degree of freedom
Dynamics
Friction

Corresponding author:

Zulfiqar A Khan
NanoCorr, Energy & Modelling (NCEM) Research Group,
Department of Design and Engineering,
Faculty of Science & Technology,
Bournemouth University, United Kingdom BH12 5BB
E-mail: zkhan@bournemouth.ac.uk

A B S T R A C T

Mission criticality in disaster search and rescue robotics highlights the requirement of specialized equipment. Specialized manipulators that can be mounted on existing mobile platforms can improve rescue process. However specialized manipulators capable of lifting heavy loads are not yet available. Moreover, effect of joint friction in these manipulators requires further analysis. To address these issues, concepts of model based design and concurrent engineering are applied to develop a virtual prototype of the manipulator mechanism. Closed loop manipulator mechanism actuated by prismatic actuators is proposed herein. The mechanics model of the manipulator is presented here as a set of equations and as multibody models. Mechanistic simulation of the virtual prototype has been conducted and the results are presented. Combined friction model that comprises Coulomb, viscous and Stribeck friction is used to compute frictional forces and torques generated at each one degree of freedom translational and rotational joints. Multidisciplinary approach employed in this work improves product design cycle time for complex mechanisms. Kinematic and dynamic parameters are presented in this paper. Friction forces and torques from simulation are also presented in addition to the visual representation of the virtual prototype.

1. INTRODUCTION

Search and rescue operation (SAR) is time critical - only a small window of opportunity exists to search out and rescue the disaster victims who are trapped [1]. Currently only a few rescue teams have access to specialized rescue robots that are durable and resilient to hazardous environments available in such disaster sites e.g. [2,3]. Durability of the robot is important because rescue sites contain abrasives, corrosive fluids and vapour-borne particulates. Robotic platforms have been proposed for carrying load e.g. [4] but manipulators that can assist rescuers to lift heavy rubble are yet to be seen. A scalable manipulator design is proposed in this work, which can be deployed with existing mobile robotic platforms.

Manipulators mechanisms can be classified as open chain [5] and closed chain manipulator [6]. The load carrying capacity of closed chain manipulator mechanism is higher compared to open chain (serial) manipulators. Also, these manipulators undergo reduced linkage flexure compared to open chain manipulator. The disadvantage of such manipulators is reduced manipulator dexterity imposed by the constraint of additional joints. Additionally, linear actuation of the manipulator can be more efficient for operations in carrying heavier payloads.

Design of the mechanism contributes substantially towards failure avoidance [7–10]. The first step in design analysis is the preparation of the kinematic model, based on body geometries [11]. Then the equation of motion (EOM) is formulated. Dynamic modelling for developing controller has been presented in [12–17]. In this work, the dynamic model of the system is modelled by using Newton Euler method. However, formulation of mathematical models of complex mechanisms is tedious and error prone. Complexity of dynamic formulation is increased by the end effector interaction with soil [17–19].

The high cost of friction forms a sizeable part of national GDP and frictional losses affect both reliability and durability of interacting systems [20–23]. Introduction of nonlinear friction which occurs in the manipulator joints further increases the model complexity. Friction is a system property that depends on factors such as materials at the contact, asperity contact, interfacial roughness, contact geometry, load acting on the contact, lubricant, mode of lubrication and operating conditions [23–28]. A review of friction in mechanism joints has been presented in [29]. Friction forces are non-linear components in the dynamics of the manipulator mechanism [30–32]. Friction in excavator manipulators with a focus on manipulator control has been previously studied [31]. In this paper, frictional forces and torques generated at joints are computed by using the combined equation for capturing the effects of Coulomb, viscous and Stribeck friction.

Another problem addressed in this paper is that of simulation parameters of the mechanism. In the past, several researchers have utilised simulation parameters which include mass properties of links in the mechanism from literature e.g. [11,33], because of the complexity of the process of deriving these parameters which increases with the complexity of link geometry. The use of computer aided design (CAD) to create virtual prototypes addresses this problem. The virtual prototype is created and simulated in multibody dynamic environments. However, mastery of CAD is tedious [34].

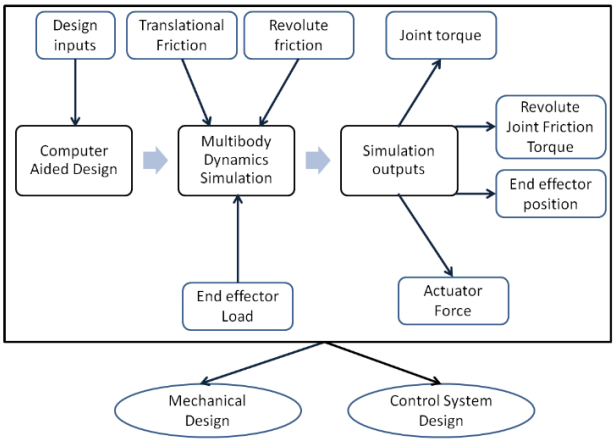

Fig. 1. Schematic of design and simulation.

The schematic of the process followed in this paper is shown in Fig. 1. Modelling and simulation improves the manipulator model for the intended application and results in reduced development cost and cycle time [35–38]. A multidisciplinary approach incorporating manipulator dynamics and joint friction models is presented in this paper. Manipulator terminology is presented in the next section.

2. SPECIFICATIONS OF THE MANIPULATOR

Manipulator design specifications have been mentioned in Table 1 which shows the parameters corresponding to each link of the manipulator linkage. Lightweight aluminium alloy (Al7075) material has been applied to the main links. These parametric values are utilized for the dynamic simulation. The terminology followed in literature [13] has been presented in Fig. 2 and in Table 1. The base and bucket links have similar mass parameters as shown in Table 1. The manipulator kinematic mechanism has been described in the following section.

Table 1 Link parameters of each link.

No.	Body	Mass (kg)	Centres of Mass (mm)		
			x	y	z
1	Base	1.29	-7.1	-66.5	0
2	Boom	3.92	84.5	215.9	0
3	Stick	0.94	101.7	4.4	0
4	Bucket	1.19	45.5	38.2	-0.5
5	Boom Actuator Base	0.6	16.6	63.4	0
6	Boom Actuator Follower	0.1	0	87.3	0
7	Stick Actuator Base	0.64	72.2	14.8	0
8	Stick Actuator Follower	0.1	0	97.3	0
9	Bucket Actuator Base	0.6	16.6	63.4	0
10	Bucket Actuator Follower	0.03	87.3	0	0

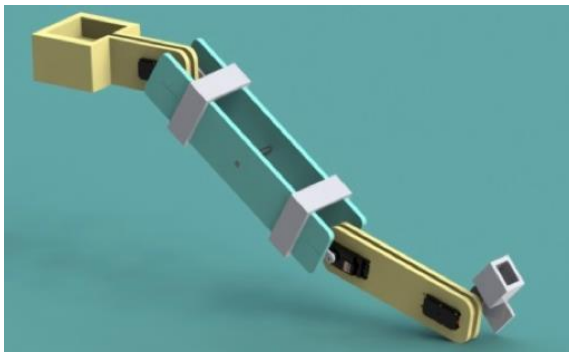

a)

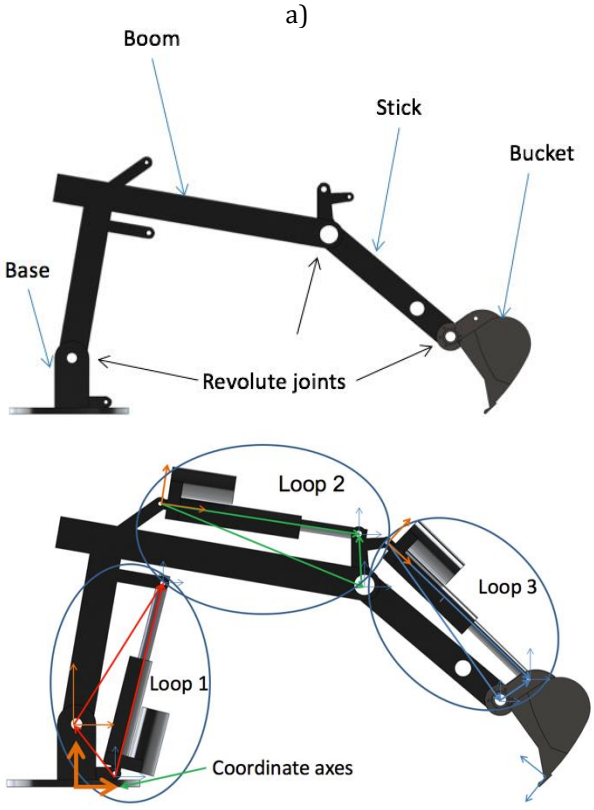

b)

Fig. 2. The above schematic shows (a) serial manipulator and (b) closed loop manipulator mechanisms.

3. MANIPULATOR MODELLING

3.1. Kinematic Modelling

The manipulator comprises three linkages joined at revolute joints having one revolute degree of freedom (Fig. 3).

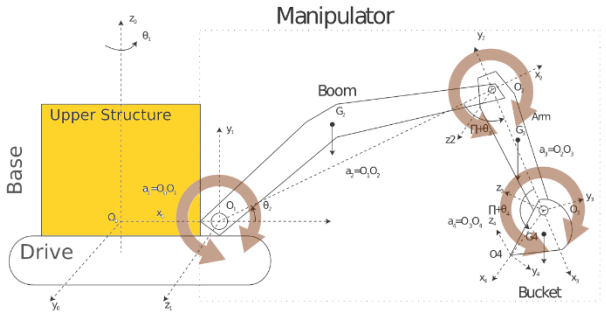

Fig. 3 Co-ordinate axis system represented using DH coordinate assignment approach [39].

The motion of the manipulator is assumed to be planar. A point on the i+1th link may be expressed in the coordinate system of the ith link can be expressed as [11]:

$$^{i}p = A_{i-1}^{i}\,{}^{i+1}p \tag{1}$$

where two-dimensional transformation matrix A_{i-1}^{i} is given by:

$$A_{i-1}^{i} = \begin{bmatrix} \cos\theta_i & -\cos\alpha_i \sin\theta_i & -\sin\alpha_i \sin\theta_i & a_i \cos\theta_i \\ \sin\theta_i & \cos\alpha_i \cos\theta_i & -\sin\alpha_i \sin\theta_i & a_i \sin\theta_i \\ 0 & \sin\alpha_i & \cos\alpha_i & d_i \\ 0 & 0 & 0 & 1 \end{bmatrix} \tag{2}$$

3.2. Equation of motion

The following equations present the recursive rotational and translational velocities and accelerations for the links [13]:

$$^{i+1}\vec{\omega}_{0(i+1)} = {}^{i+1}\vec{\omega}_{0i} + \dot{\theta}_{i+1}({}^{i+1}\vec{k}_{zi}) \tag{3}$$

$$^{i+1}\vec{\alpha}_{0(i+1)} = {}^{i+1}\vec{\alpha}_{0i} + \ddot{\theta}_{i+1}({}^{i+1}\vec{k}_{zi}) \tag{4}$$

$$^{i+1}\vec{v}_{0(i+1)} = {}^{i+1}\vec{v}_{0i} + {}^{i+1}\vec{\omega}_{0(i+1)} \times [{}^{i+1}\vec{p}_{0(i+1)} - {}^{i+1}\vec{p}_{0i}] \tag{5}$$

$$\begin{aligned} {}^{i+1}\vec{a}_{0(i+1)} = {}^{i+1}\vec{a}_{0i} + [{}^{i+1}\vec{\alpha}_{0(i+1)} \times ({}^{i+1}\vec{p}_{0(i+1)} - {}^{i+1}\vec{p}_{0i})] \\ + {}^{i+1}\vec{\omega}_{0(i+1)} \times [{}^{i+1}\vec{\omega}_{0(i+1)} \times ({}^{i+1}\vec{p}_{0(i+1)} - {}^{i+1}\vec{p}_{0i})] \end{aligned} \tag{6}$$

Eq. (3) represents the angular velocity of the origin of the i+1th frame represented in the i[th] frame and eq. (4) presents the angular acceleration of the same. Similarly, translational velocity and acceleration are given in Eq (5) and (6). The rotational and translational kinematic parameters of the centres of gravity of the links can be expressed as follows [13]:

$$^{i+1}\vec{v}_{0G_i} = {}^{i}\vec{v}_{0i} + {}^{i+1}\vec{\omega}_{0i} \times [\vec{p}_{0G_i} - \vec{p}_{0i}] \quad (7)$$

$$^{i+1}\vec{a}_{0G_i} = {}^{i}\vec{a}_{0i} + {}^{i}\vec{\alpha}_{0i} \times [\vec{p}_{0G_i} - \vec{p}_{0i}] + {}^{i}\vec{\omega}_{0i} \times [{}^{i}\vec{\omega}_{0G_i} \times (\vec{p}_{0G_i} - \vec{p}_{0i})] \quad (8)$$

3.3. Dynamic Analysis

In this section, the dynamic analysis of the links and the dynamics equation have been presented.

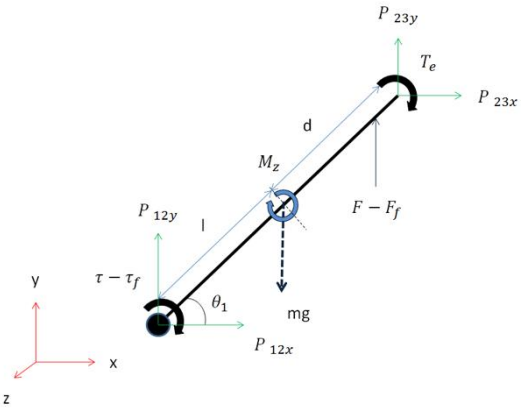

Fig. 4. Forces and moments acting on link 1 with one degree of freedom joint at the base.

The dynamic analysis of links is derived from first principles as shown in Fig. **4**. The general form of Newton's equation can be expressed as [40]:

$$\sum F = m\dot{v} = ma \quad (9)$$

where F represents the resultant external force, m is the mass of the link, v is the velocity of the centre of mass.

For a planar manipulator, the recursive relation can be expressed as [13]:

$$^{i}F_0^i = m_i \, {}^{i}a_{0G_i} \quad (10)$$

The general form of the Euler equation for a rigid body undergoing rotation is expressed as [40]:

$$\sum \tau = I\dot{\omega} = I\alpha \quad (11)$$

For a planar manipulator, the recursive relation angular momentum relationship can be expressed as [13]:

$$^{i}\vec{M}_0^i = {}^{i}I_{0i} \, {}^{i}\vec{\omega}_0^i + {}^{i}\vec{\omega}_{0i} \times {}^{i}I_{0i}({}^{i}\vec{\omega}_{0i}) \quad (12)$$

where M is the torque and I is the central moment of inertia.

The combined Newton Euler equation can be expressed in the form given below based on [13]:

$$D(\theta)\ddot{\theta} + H(\theta,\dot{\theta})\dot{\theta} + G(\theta) + B(\dot{\theta}) = \tau - \tau_L \quad (13)$$

where

$$D(\theta) = \begin{bmatrix} D_{11} & D_{12} & D_{13} & D_{14} \\ D_{21} & D_{22} & D_{23} & D_{24} \\ D_{31} & D_{32} & D_{33} & D_{34} \\ D_{41} & D_{42} & D_{43} & D_{44} \end{bmatrix}$$

$$C(\theta,\dot{\theta}) = \begin{bmatrix} C_{11} & C_{12} & C_{13} & C_{14} \\ C_{21} & C_{22} & C_{23} & C_{24} \\ C_{31} & C_{32} & C_{33} & C_{34} \\ C_{41} & C_{42} & C_{43} & C_{44} \end{bmatrix}$$

$$G(\theta) = \begin{bmatrix} G_1 & G_2 & G_3 & G_4 \end{bmatrix}$$

where θ represents joint angles (n x 1 matrix), n represents the number of main links and $\dot{\theta}$, $\ddot{\theta}$ represents the angular velocity and angular accelerations, $D(\theta)$ represents pseudo inertia matrix, $C(\theta,\dot{\theta})$ represents Coriolis' and centripetal forces, $G(\theta)$ represents gravity forces, $B(\dot{\theta})$ represents joint frictional forces, τ represents the joint torques, τ_L represents interaction forces at the end effector between machine and environment i.e. soil.

For simplicity, Alekseeva model has been substituted with a constant load (F_T=F_N= 150N). Inverse dynamics simulation is conducted i.e. input consist of angular parameters and their derivatives with respect to time, and the output is the forces and torques. Friction force has been computed at the revolute and prismatic joints by using models presented in a later section.

4. FRICTION MODEL

4.1. Translational friction

Translational friction model for the actuation is described below. The parameters have been listed as follows: Total friction force F is computed during the simulation, Coulomb friction force $F_c = 20N$, breakaway friction force $F_{\text{brk}} = 25N$, coefficient $c_v = 100N/(m/s)$, threshold friction value 24.995Nm and velocity threshold $v_{thr} = 1e-4m/s$. Translational friction as a combination of Stribeck, Coulomb and viscous friction can be expressed by the following equations [41,42]:

$$F_f = F_c + F_{brk}.\exp((-c_v|v|))\text{sign}(v) + fv \quad (14)$$

$$F_f = \frac{v}{v_{thr}}(fv_{vt} + F_C + (F_C - F_{brk}).\exp(-c_v|v_{thr}r|))\text{sign}(-c_v v_{thr}) + fv_{thr}) \quad (15)$$

where $v = v_R - v_c$.

4.2. Revolute friction model

Combined revolute friction model comprising Coulomb, viscous and Stribeck friction are described by equations (16-17). Friction torque τ_f is computed by using a switching model equation represented by Eq. 13 and 14 which is based on a threshold velocity value that is determined through tribo-experimentation. The values of Coulomb friction torque τ_C is assumed to be 20 Nm, breakaway friction torque τ_{brk} is 25 Nm, the coefficient $c_v = 0.001N.m.s/rad$, threshold velocity $\omega_{th} = 1e-4rad/s$ and the threshold torque $\tau_{\text{brk}} = 24.995\,\text{Nm}$. The conditional equations for generated friction torque at the joints of the manipulator are given by [43]:

$$\tau_f = (\tau_C + (\tau_{\text{brk}} - \tau_C).\exp(-c_v|\omega|))\text{sign}(\omega) + f\omega \quad (16)$$

$$\tau_f = \frac{\omega}{\omega_{thr}}(\tau_C + (\tau_{\text{brk}} - \tau_C).\exp(-c_v|\omega_{th}r|))\text{sign}(-c_v\omega_{th}) + f\omega_{thr}) \quad (17)$$

5. MODEL BASED REPRESENTATION OF MANIPULATOR MECHANICS

The manipulator mechanistic model represented in the form of Eq. (1-8) and (12-13) can be presented by the model based block diagram (see Fig. 5). The mechanism configuration block contains the magnitude and direction settings of the gravity force in the simulation environment. The 'environment' and 'root/ground' blocks are replaced by the 'World' block, the 'mechanism configuration' block and the 'Solver' block. Transformation frames are used to connect various bodies to each other and joints in lieu of direct connections, through separate physical signals. The solid block represents each body, is connected to this signal and contains editable data that is inherited from the CAD virtual prototype including the mass of the body, centre of mass, moments of inertia and products of inertia. For logging the signals generated in the system, the native physical signal, green coloured lines in Fig. 6, are required to be converted to Simulink signals by using a conversion block. Similarly, the converse process for the input signals to the joints and the converted signals can be displayed by using a 'Scope' block. Selection of explicit forward/inverse dynamics or kinematics mode selection is not required for this type of simulation.

The computation of dynamic parameters is evaluated from the joint block. Selection of the appropriate numerical solver will ensure simulation accuracy. Numerically stiff solvers use more steps when rapid change in parameter value occurs. In friction models, the problem of zero crossing is encountered at the change of velocity direction and this is addressed by using the conditional/switching model represented by equations (14-17). The simulation block diagrams for two different simulation platforms have been presented in Fig. 6.

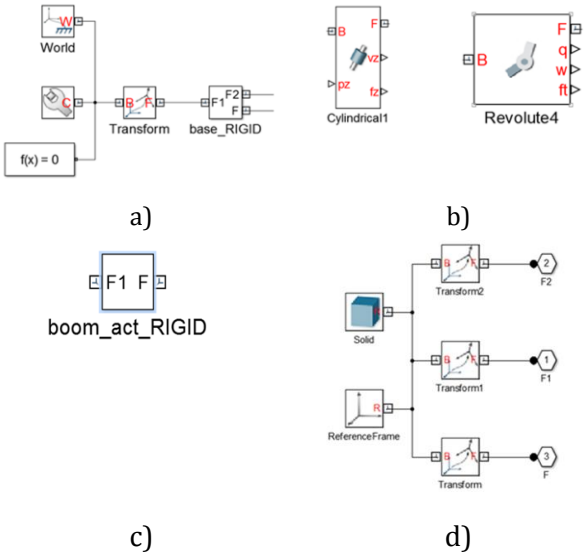

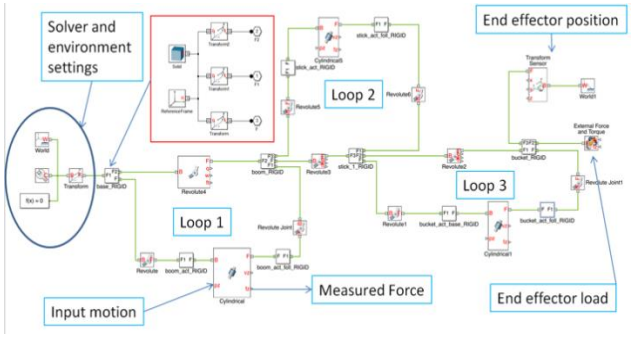

e)

Fig. 5. (a) Global coordinate system, environment and solver settings, (b) Cylindrical joint block and Revolute Joint block (c) Body block (d) Components of the body block including transformation frames (e) Multibody dynamics simulation showing the bodies, joints, sensors, external loads, global coordinate system, solver block and transform block.

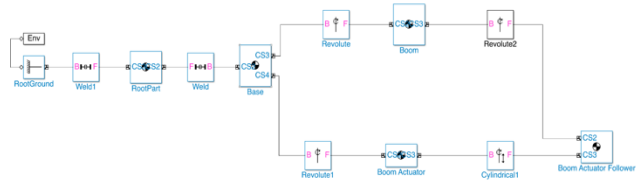

a)

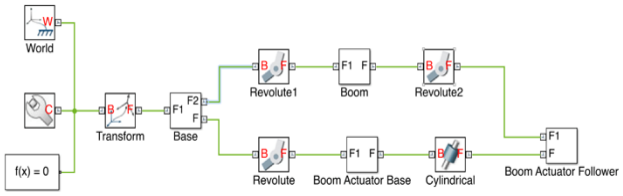

b)

Fig. 6. The model based graphical visualization form of the first loop of the manipulator mechanism (a) for first generation type simulation and (b) for second generation simulation.

5.1. Simulation Input

Input to the simulation model is shown in Fig. 7. The signal builder block is used to generate the motion input signal. The three blocks represent the base signal, the first and second time differentials of the input signals respectively. The transfer function is chosen according to [44] in order to overcome the abrupt changes to velocity and acceleration which would have occurred if a simple differential function was used. In other words, the differential curves are smoothed thus avoiding singularities in time differentials, which lead to more accurate simulations. Results of simulations are presented in Section 6.

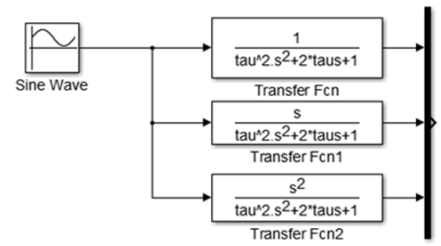

a)

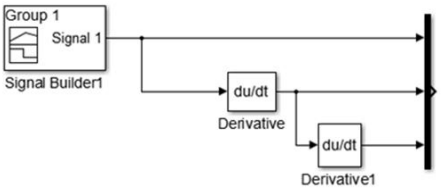

b)

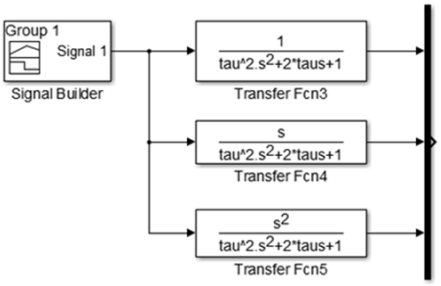

c)

Fig. 7. The input function uses a transfer function based differentiation method where the parameter tau can be adjusted.

6. RESULTS

Input signals are shown in Figs. (8-11). Comparison of two simulations are shown in Fig. 12. Output parameters recorded from the simulation include the revolute joint parameters i.e. the revolute angles and its derivatives: velocity and acceleration are shown in Fig. 13, Fig. 14 and Fig. 15 (a-e). The translational actuator forces and friction forces computed using eq. (14-15) are represented in Fig. 16, Fig. 17 and Fig. 18. Results for translational actuator for simulation 3 (a-b) dynamic parameters
. The values of peak revolute joint torque are given by -0.2884 Nm and -0.05511 Nm at 0.1995 s and 0.181 s respectively for joints 1 and 3. The torque for joint 3 remains unaffected owing to constant external load. From the combined equation for revolute friction, values of the revolute joint torque are given by 27.63Nm for joint 3, 27.56 Nm for joint 2 and 23.69Nm for joint 3 at 0.103, 0.103 and 0.968 seconds respectively. The inflexion values at the crest and trough for the translational actuator force

are given by -1.094 N, -0.8348 N and 0.7819 N at 3.635, 3.404 and 3.7 s respectively are the ordered pairs for simulation time and magnitude of force in newton.

Mechanics explorer window displaying the simulation, the table on the left shows the model tree (e.g. base, boom etc.) is presented in Fig. 19.

The four windows on the right display different views of the manipulator mechanism. The centres of gravity and the coordinate axis assignments for each joint of the mechanical linkage in the 'mechanics explorer' window can be displayed (Fig. 19). The conclusions from this study are presented in the next section.

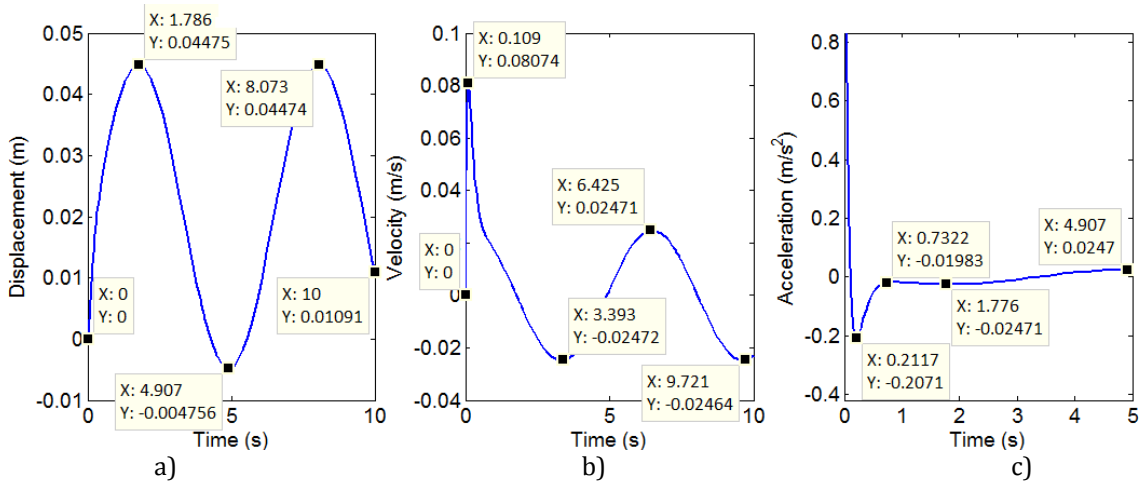

a) b) c)

Fig. 8. Actuator input signal: Amplitude = 0.025, Bias = 0.02, Frequency = 1 rad/sec, the velocity and acceleration are derivatives of the main input signal.

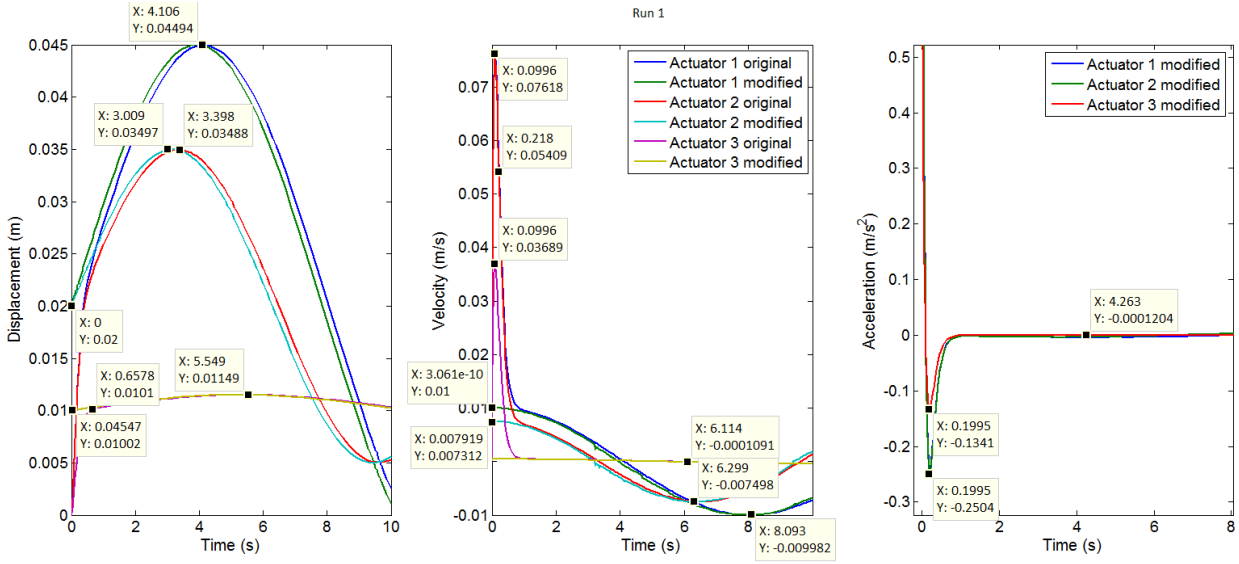

a) b) c)

Fig. 9. Input parameters for simulation 1: amplitude a1 = 0.025, bias = 0.02, frequency = 0.4 rad/sec, amplitude a2 = 0.015, bias = 0.02, frequency= 0.5 rad/sec, amplitude a3 = 0.0015, bias = 0.01, frequency= 0.3 rad/sec, the original signal assumes tau = 0.1, the modified signal assumes tau = 0.01.

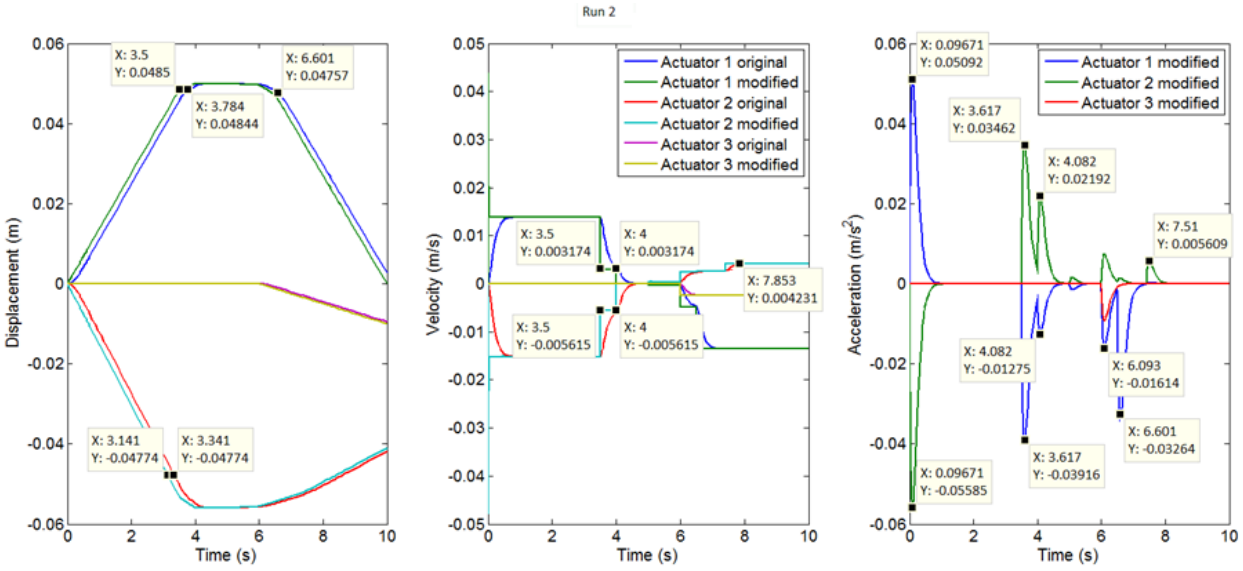

a) b) c)

Fig. 10. Simulation input signal parameter tau = 0.1 to achieve realistic dig pattern.

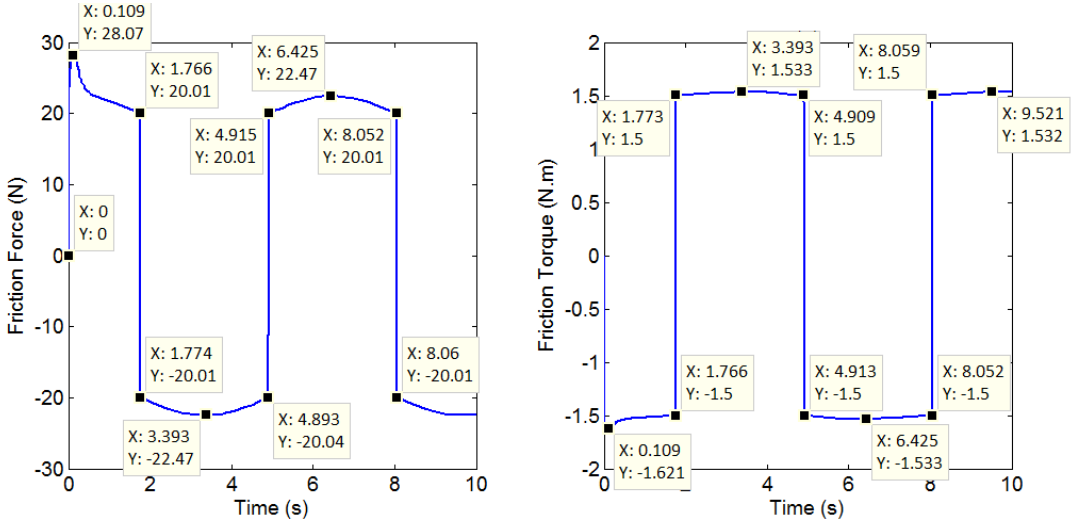

Fig. 11. Simulation 3 with custom input signal to achieve realistic dig pattern, tau = 0.01.

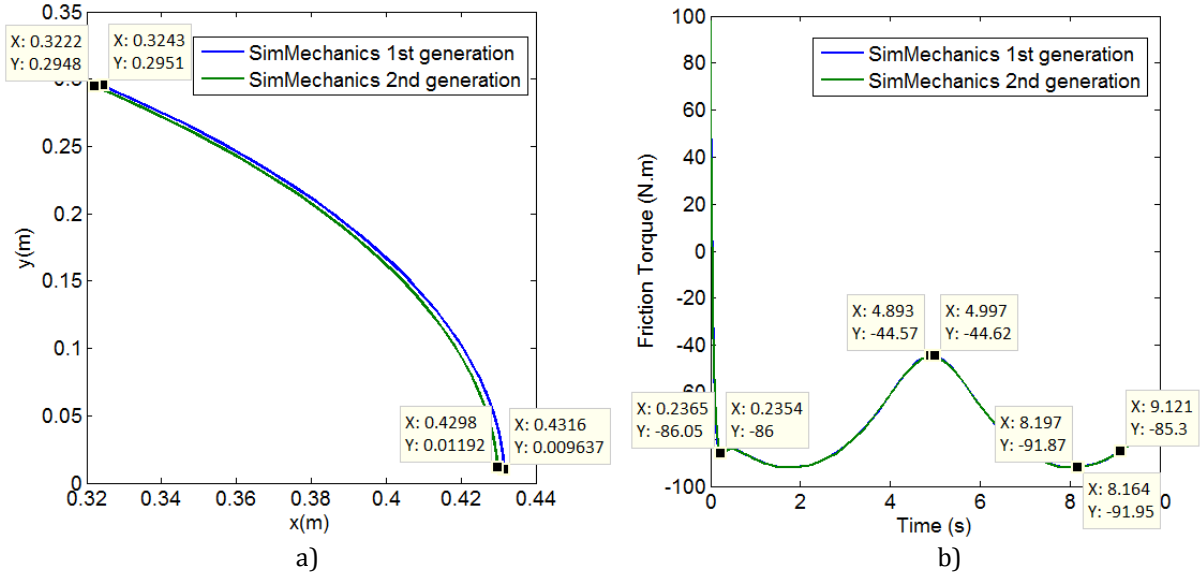

a) b)

Fig. 12. Comparison of (a) End effector motion in two-dimensional space, (b) Friction torque generated at the revolute joint, using SimMechanics 1st and 2nd Generation simulations.

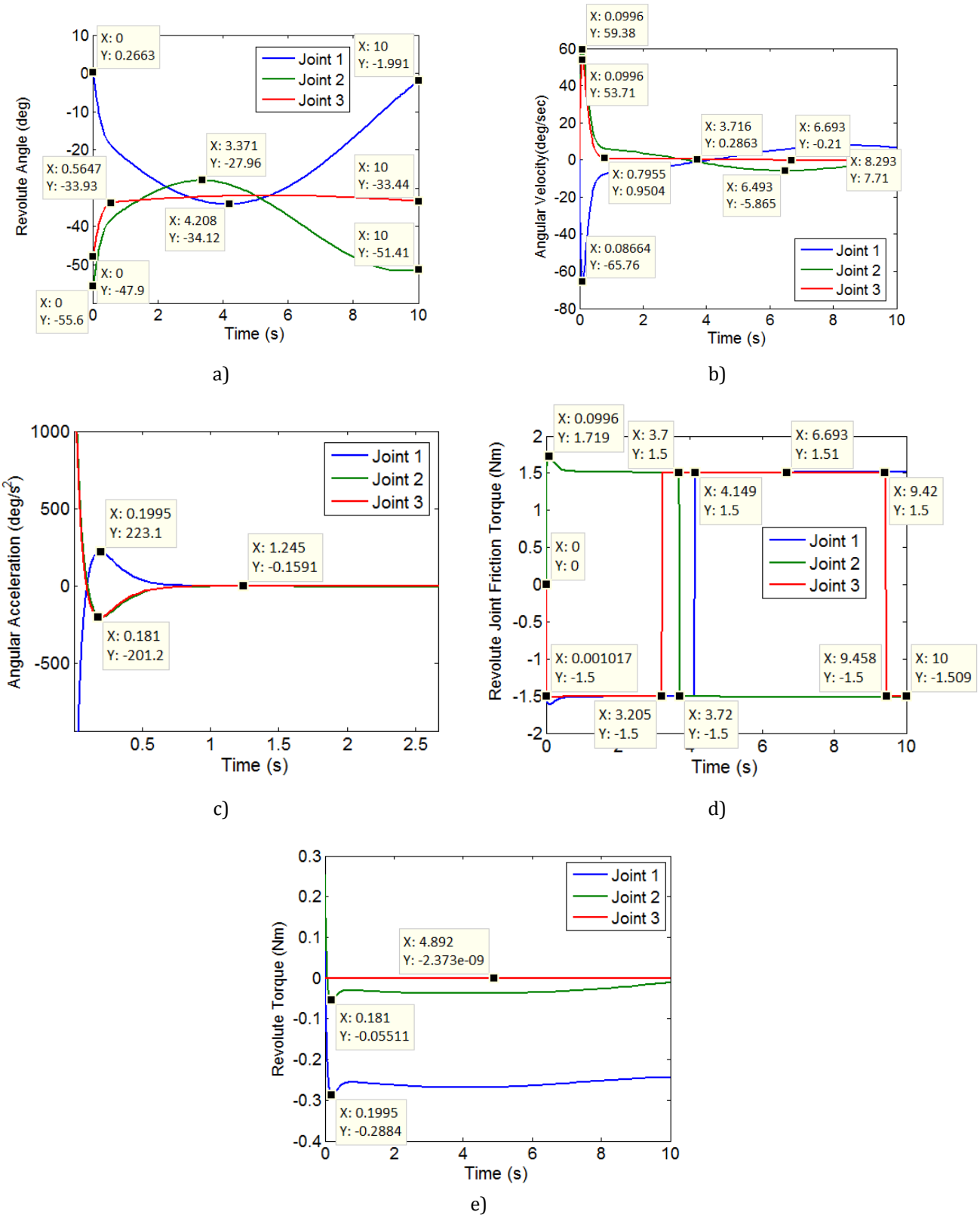

Fig. 13. Results for revolute joint for simulation 1 (a-c) Joint kinematic parameters (d-e) dynamic parameters.

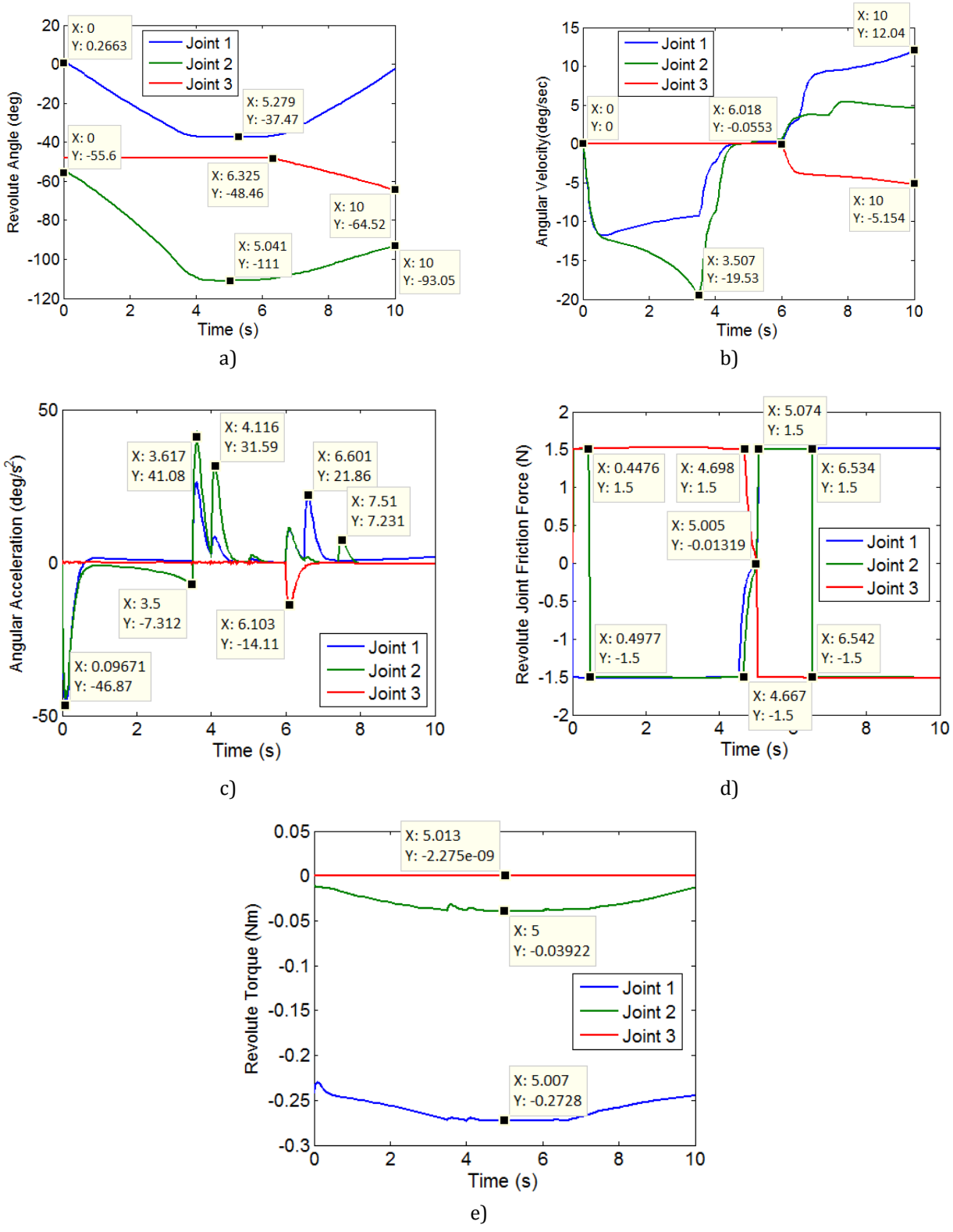

Fig. 14. Results for revolute joints for simulation 2 1 (a-c) Joint kinematic parameters (d-e) dynamic parameters.

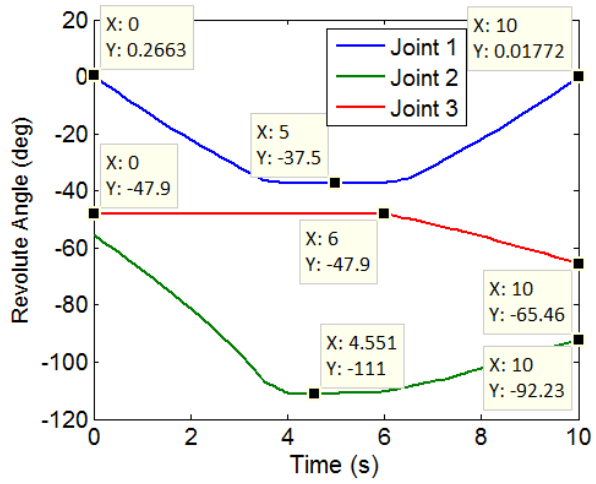

a)

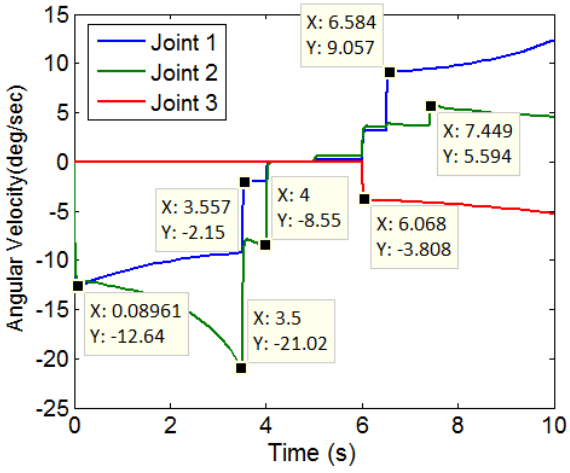

b)

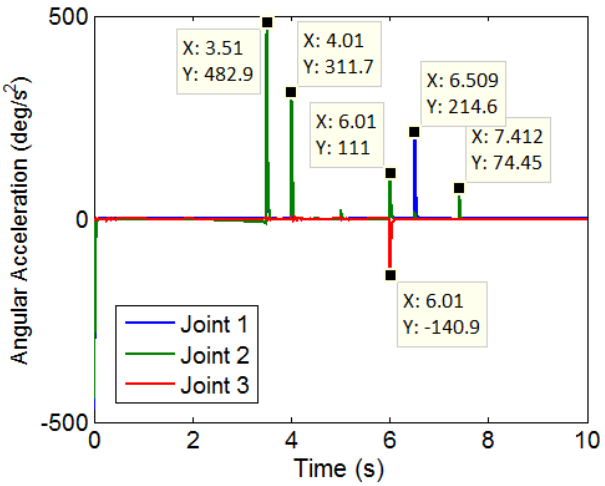

c)

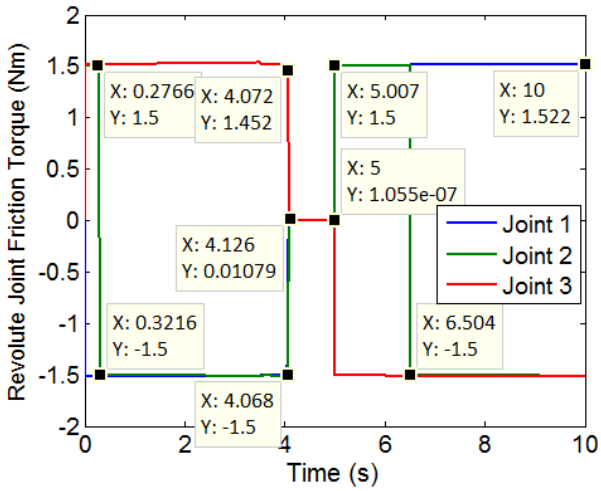

d)

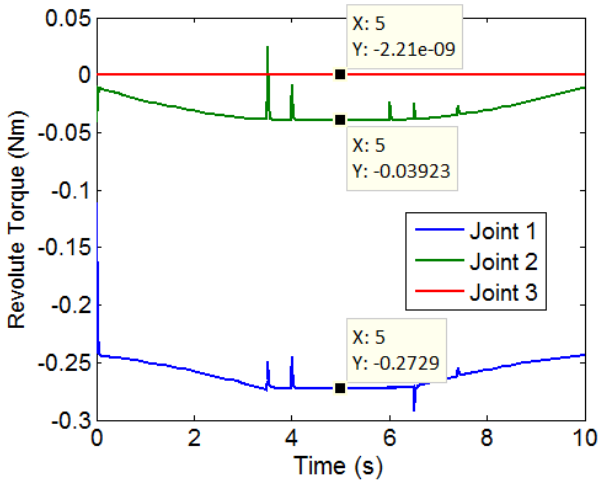

e)

Fig. 15. Results for revolute joints for simulation 3 1 (a-c) Joint kinematic parameters (d-e) dynamic parameters.

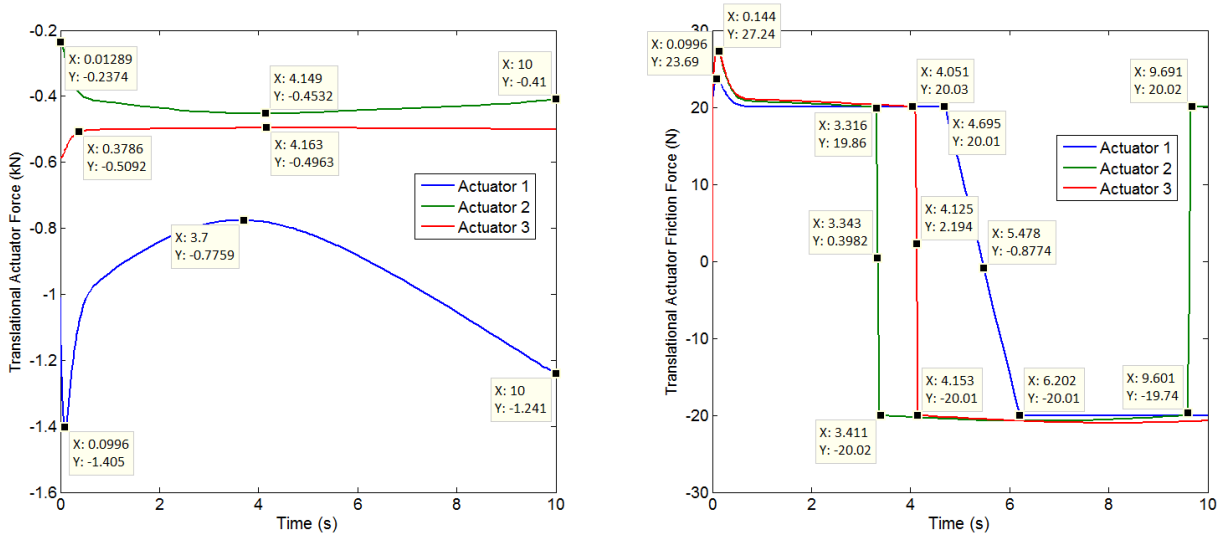

a) b)

Fig. 16. Results for translational actuator for simulation 1 1 (a-b) dynamic parameters

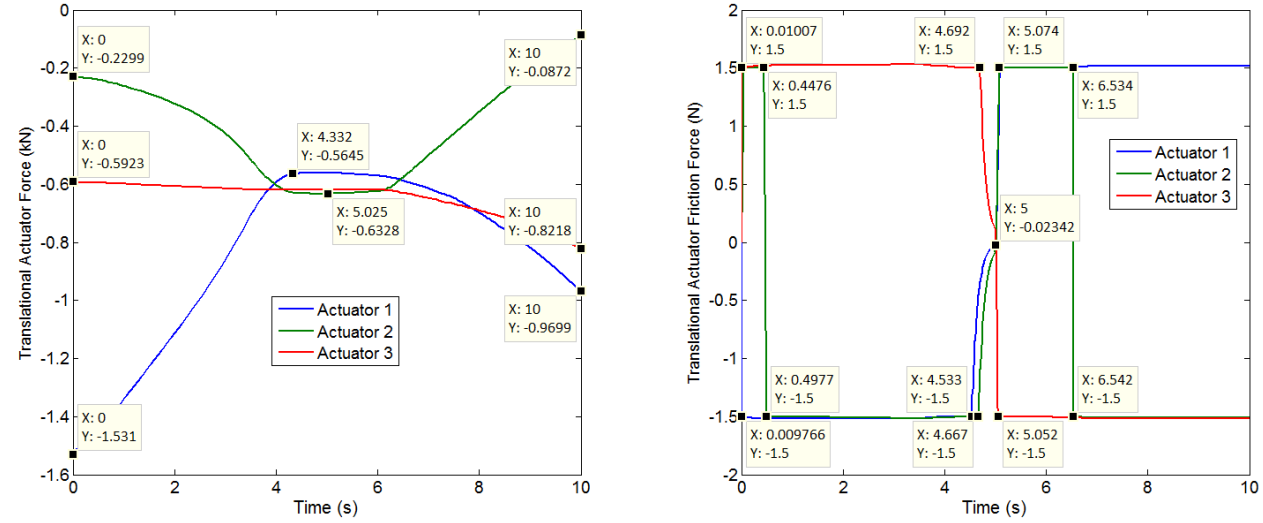

a) b)

Fig. 17. Results for translational actuator for simulation 2 (a-b) dynamic parameters.

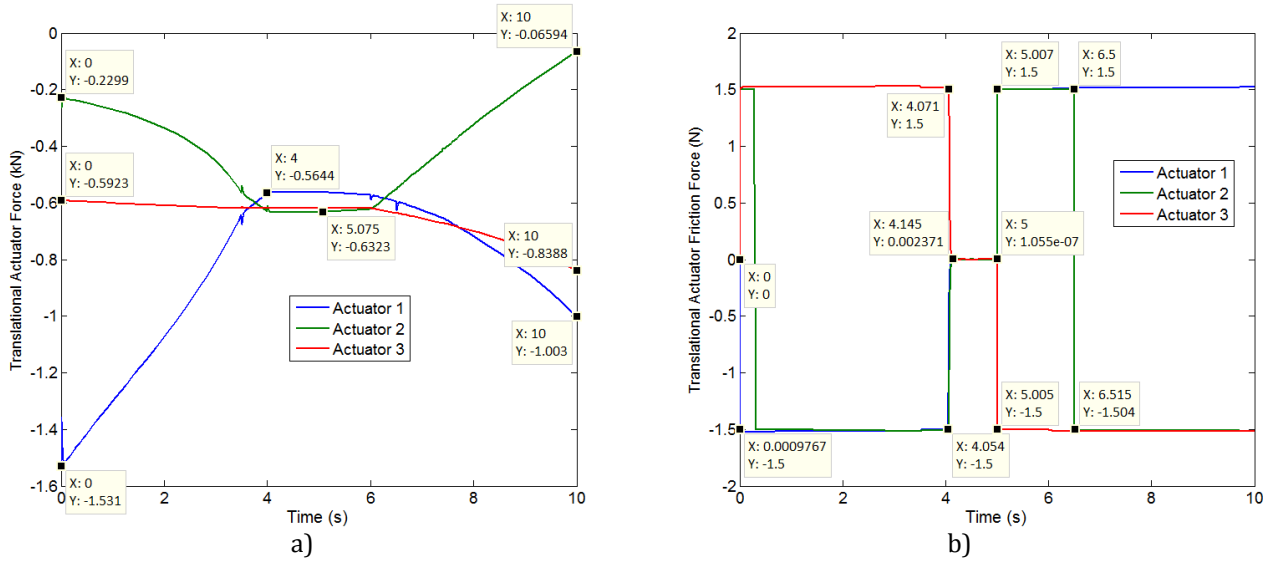

a) b)

Fig. 18. Results for translational actuator for simulation 3 (a-b) dynamic parameters

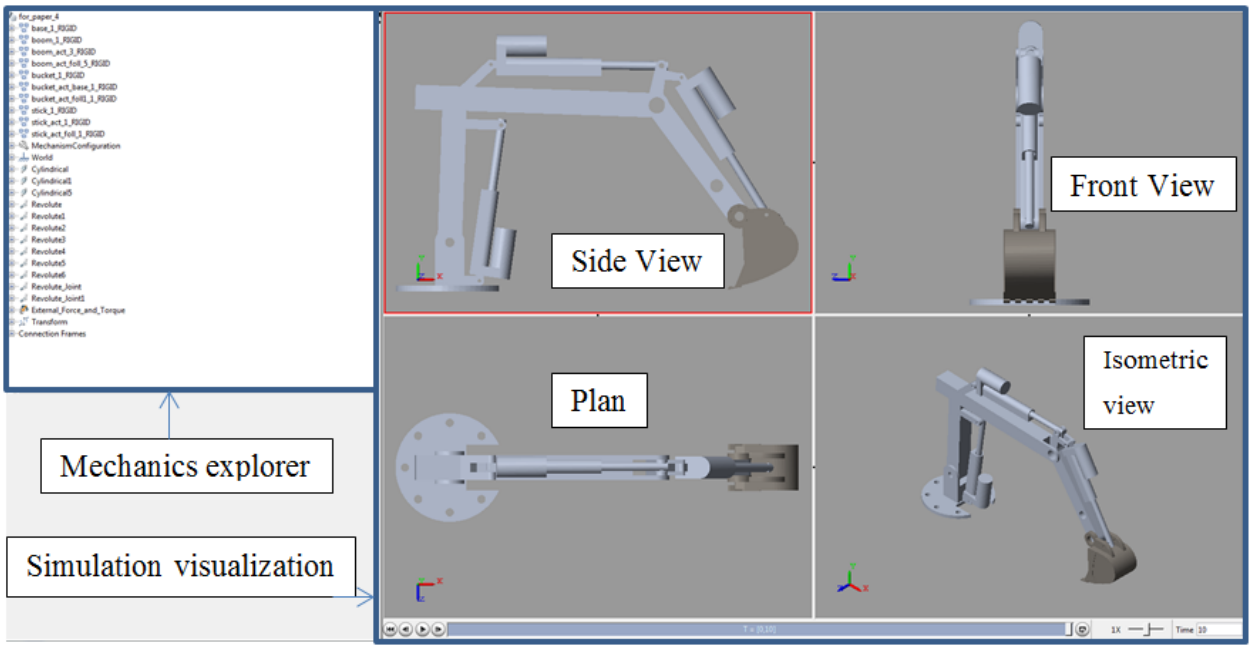

Fig. 19. Mechanics Explorer showing the dynamic simulation views.

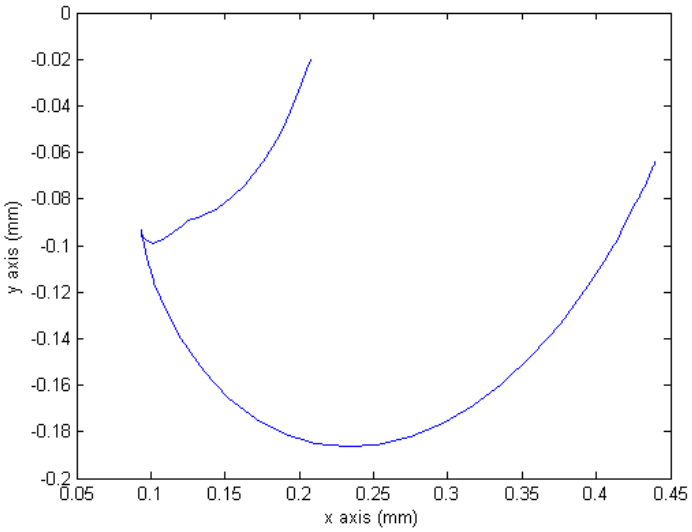

Fig. 20. End effector trajectory in planar space.

7. CONCLUSION

The process of development of mechanistic models of complex manipulator systems is highly challenging. The design and mechanistic simulation of a mobile manipulator is presented in this paper. Computer aided design and multibody simulation method has been utilised in this work to conduct mechanistic simulation of the model. Friction in joints of links affects the performance of manipulator mechanism. The estimation of friction force in manipulator mechanisms is often overlooked. However, for manipulators requiring precise positioning and stable operation, friction force needs to be computed. The first step towards estimating joint friction force is to use a combined friction model for translational and revolute joints.

In this paper, novel simulation method for mechanisms using virtual prototyping in CAD has been presented, which accelerates the start to production design cycle thereby enabling rapid design iterations. Mechanistic parameters including kinematic parameters such as joint displacement, velocity and acceleration,

corresponding to the input are plotted, in addition to the dynamic parameters for actuation and friction of the mechanism. The advantages of utilising this method can be summed up as follows: It offers (1) increased accuracy of computation of link parameters such as mass, moment of inertia, centres of gravity and radius of gyration for complex links' shapes, (2) ease of assemblage of the mechanism, (3) assignment of relationship between links of the overall mechanism, (4) ease of visual examination of coordinate systems, (5) capability to visually validate manipulator motion and checking for interference of links without incurring the additional cost of fabricating the physical prototype, (6) design refinement of the mechanism including modification of design, material assignment, leading to shorter product development cycles, (7) diagrammatic representation of CAD model in the multibody dynamics environment, (8) load on end effector, which can be applied and validated, and (9) virtual prototype can be used for the design and testing of controller and extended to hardware in the loop (HIL) simulation for testing. Compared to numerical equation modelling, this approach has the advantages of time saving and visual simulation aspect and enabling the use of concurrent engineering technique. Moreover, the modelling of complicated linkages is made possible, along with the dynamic simulation and application of external load. Parameter variations of intermediate links can easily be incorporated and simulated. Friction forces at translational sliding and revolute joints are computed based on modified combined friction equation.

8. FUTURE WORK

Simulation of the virtual prototype in the multibody dynamics simulation environment can be extended to a three-dimensional motion through the addition of an appropriate robot platform for the base, resulting in the simulation of a full-fledged robotic platform. Alternative end-effector designs such as a grappling attachment or hand [5] can be rapidly developed and added to the existing virtual prototype, which can be utilized to test and develop the control system for the robot.

In addition, the results from dynamic simulation can be used for further analysis of the link by using analytical tools such as finite element analysis to ensure reliable design. Friction and wear phenomenon in the joints will be investigated by using tribo-testing [45] techniques and joint surface engineering will be suggested to improve friction and wear properties of the contacting surface.

REFERENCES

[1] A. L. Adams *et al.*, "Search Is a Time-Critical Event: When Search and Rescue Missions May Become Futile," *Wilderness Environ. Med.*, vol. 18, no. 2, pp. 95–101, 2007.

[2] A. Hirayama and K. Ito, "Development of rescue manipulator to search narrow space for victims," *Artif. Life Robot.*, vol. 13, no. 1, pp. 331–335, 2008.

[3] V. Chacko, H. Yu, S. Cang, and L. Vladareanu, "State of the art in excavators," *Proc. 2014 Int. Conf. Adv. Mechatron. Syst.*, pp. 481–488, 2014.

[4] M. Raibert, K. Blankespoor, G. Nelson, and R. Playter, "BigDog, the Rough-Terrain Quadruped Robot," *IFAC Proc. Vol.*, vol. 41, no. 2, pp. 10822–10825, 2008.

[5] A. Khurshid, K. Zulfiqar, V. Chacko, A. Ghafoor, M. A. Malik, and Y. Ayaz, "Modelling and Simulation of a Manipulator with Stable Viscoelastic Grasping Incorporating Friction," *Tribol. Ind.*, vol. 38, no. 4, pp. 559–574, 2016.

[6] K. Waldron, J. Schmiedeler, K. Waldron, J. Schmiedeler, and J. Schmiedeler, "Kinematics," *Springer Handb. Robot.*, pp. 9–33, 2008.

[7] R. R. Murphy, "Trial by fire [rescue robots]," *Robot. Autom. Mag. IEEE*, vol. 11, no. 3, pp. 50,61, 2004.

[8] J. A. Kramer and R. R. Murphy, "Endurance testing for safety, security and rescue robots," *Perform. Metrics Intell. Syst.*, 2006.

[9] J. Carlson and R. R. Murphy, "Reliability analysis of mobile robots," *2003 IEEE Int. Conf. Robot. Autom. (Cat. No.03CH37422)*, vol. 1, pp. 274–281, 2003.

[10] S. Shah and A. Guha, "Bearing Health Monitoring," *Tribol. Ind.*, vol. 38, no. 3, pp. 297–307, 2016.

[11] A. J. Koivo, "Kinematics of Excavators (Backhoes) for Transferring Surface Material," *J. Aerosp. Eng.*, vol. 7, no. 1, pp. 17–32, 1994.

[12] P. K. Vähä and M. J. Skibniewski, "Dynamic Model

of Excavator," *J. Aerosp. Eng.*, vol. 6, no. 2, pp. 148–158, 1993.

[13] A. J. Koivo, M. Thoma, E. Kocaoglan, and J. Andrade-Cetto, "Modeling and Control of Excavator Dynamics during Digging Operation," *J. Aerosp. Eng.*, vol. 9, no. 1, pp. 10–18, 1996.

[14] T. Makkonen, K. Nevala, and R. Heikkilä, "A 3D model based control of an excavator," *Autom. Constr.*, vol. 15, no. 5, pp. 571–577, 2006.

[15] S. Singh, "State of the Art in Automation of Earthmoving," *J. Aerosp. Eng.*, vol. 10, no. 4, pp. 179–188, 1997.

[16] J. a. Marshall, P. F. Murphy, and L. K. Daneshmend, "Toward Autonomous Excavation of Fragmented Rock: Full-Scale Experiments," *Autom. Sci. Eng. IEEE Trans.*, vol. 5, no. 3, pp. 562–566, 2008.

[17] D. Seward, F. Margrave, I. Sommerville, and R. Morrey, "LUCIE the robot excavator-design for system safety," *Proc. IEEE Int. Conf. Robot. Autom.*, vol. 1, no. April, pp. 963–968, 1996.

[18] S. Singh, "Learning to predict resistive forces during robotic excavation," *Proc. 1995 IEEE Int. Conf. Robot. Autom.*, vol. 2, pp. 2102–2107, 1995.

[19] H. Cannon and S. Singh, "Models for Automated Earthmoving," *Exp. Robot. VI, Lect. Notes Control Inf. Sci.*, 1999.

[20] P. C. Mishra, "A Review of Piston Compression Ring Tribology," *Tribol. Ind.*, vol. 36, no. 3, pp. 269–280, 2014.

[21] E. Rabinowicz, "The Intrinsic Variables affecting the Stick-Slip Process," *Proc. Phys. Soc.*, vol. 71, no. 4, p. 668, 1958.

[22] P. J. Blau, "Fifty years of research on the wear of metals," *Tribol. Int.*, vol. 30, no. 5, pp. 321–331, 1997.

[23] P. J. Blau, "Introduction," *Frict. Sci. Technol.*, pp. 1–16, Oct. 2008.

[24] N. K. Myshkin and A. Y. Grigoriev, "Roughness and texture concepts in tribology," *Tribol. Ind.*, vol. 35, no. 2, pp. 97–103, 2013.

[25] Z. A. Khan, A. Saeed, O. Gregory, and A. Ghafoor, "Biodiesel performance within internal combustion engine fuel system - A review," *Tribol. Ind.*, vol. 38, no. 2, pp. 197–213, 2016.

[26] S. Senhadji, F. Belarifi, and F. Robbe-Valloire, "Experimental Investigation of Friction Coefficient and Wear Rate of Brass and Bronze under Lubrication Conditions," *Tribol. Ind.*, vol. 38, no. 1, pp. 102–107, 2017.

[27] S. Bhaumik and S. D. Pathak, "Effect of Nano and Micro Friction Modifier Based Lubricants on Wear behavior between Steel-Steel Contacts," *Tribol. Ind.*, vol. 39, no. 1, pp. 136–143, 2017.

[28] H. K. Trivedi and D. V. Bhatt, "Effect of Lubricating Oil on Tribological behaviour in Pin on Disc Test Rig," *Tribol. Ind.*, vol. 39, no. 1, pp. 90–99, 2017.

[29] Z. A. Khan, V. Chacko, and H. Nazir, "A review of friction models in interacting joints for durability design," *Friction*, vol. 5, no. 1, pp. 1–22, 2017.

[30] J. J. Craig, P. Hsu, and S. S. Sastry, "Adaptive Control of Mechanical Manipulators," *Int. J. Rob. Res.*, vol. 6, no. 2, pp. 16–28, 1987.

[31] S. T. Bilandi, "Identification of frictional effects and structural dynamics for improved control of hydraulic manipulators," The University of British Columbia, 1997.

[32] L. Simoni, M. Beschi, G. Legnani, and V. Antonio, "Friction Modeling with Temperature Effects for Industrial Robot Manipulators," *2015 IEEE/RSJ Int. Conf. Intell. Robot. Syst.*, pp. 3524–3529, 2015.

[33] P. . Vaha *et al.*, "Excavator dynamics and effect of soil on digging," *Proc. 8th ISARC, Stuttgart, Ger.*, pp. 297–306, 1991.

[34] Y. Bodein, B. Rose, and E. Caillaud, "A roadmap for parametric CAD efficiency in the automotive industry," *CAD Comput. Aided Des.*, vol. 45, no. 10, pp. 1198–1214, 2013.

[35] S. H. H. Choi and A. M. M. Chan, "A virtual prototyping system for rapid product development," *CAD Comput. Aided Des.*, vol. 36, pp. 401–412, 2004.

[36] M. I. C. Dede and S. Tosunoglu, "Virtual Rapid Robot Prototyping Florida International University Department of Mechanical Engineering 10555 West Flagler Street," *ASME Early Career Tech. J.*, vol. 5, no. 1, pp. 1–8, 2006.

[37] S. H. Choi and H. H. Cheung, "A versatile virtual prototyping system for rapid product development," *Comput. Ind.*, vol. 59, no. 5, pp. 477–488, 2008.

[38] M. Karkee, B. L. Steward, A. G. Kelkar, and Z. T. Kemp, "Modeling and real-time simulation architectures for virtual prototyping of off-road vehicles," *Virtual Real.*, vol. 15, no. 1, pp. 83–96, 2011.

[39] V. Chacko and H. Yu, "Multi-body simulation methods for rigid manipulators," *Eurathlon/SHERPA*. 2015.

[40] E. Stoneking, "Newton-Euler Dynamic Equations of Motion for a Multi-Body Spacecraft," in *AIAA Guidance, Navigation and Control Conference and*

Exhibit, 2007.

[41] V. van Geffen, "A study of friction models and friction compensation," 2009.

[42] The Mathworks Inc. UK, "Translational Friction," *Mathworks Documentation*, 2015. [Online]. Available: http://uk.mathworks.com/help/physmod/simscape/ref/translationalfriction.html.

[43] The Mathworks Inc. UK, "Rotational Friction," *Mathworks Documentation*, 2015. [Online]. Available: http://uk.mathworks.com/help/physmod/simscape/ref/rotationalfriction.html?s_tid=gn_loc_drop.

[44] G. Rouleau, "Applying Motion to SimMechanics Models," *Mathworks Blogs - Guy and Seth on Simulink*. 2012.

[45] N. K. Myshkin, "Devices for Tribotests at Micro/Nano Scale," *Tribol. Ind.*, vol. 26, no. 3–4, pp. 15–20, 2004.

NOMENCLATURE

a_i	Length of link *i*
${}^{i+1}\vec{a}_{0i}$	Linear acceleration of ith coordinate in the *i*+1th coordinate system
${}^{i+1}\vec{a}_{0G_i}$	Linear acceleration of centre of gravity of ith coordinate in the *i*+1th coordinate system
A_{i-1}^{i}	Transformation matrix
B	Frictional Torque matrix
CAD	Computer Aided Designing
CAE	Computer Aided Engineering
c_v	Coefficient
$C(\theta,\dot{\theta})$	Coriolis/Centripetal force matrix
d_i	Distance between two adjacent links
$D(\theta)$	Inertia matrix
EOM	Equations of motion
f	Viscous friction coefficient
F	Friction force
F_{brk}	Breakaway friction
F_C	Coulomb friction
${}^{i}F_0^{i}$	Force acting on the centre of the link expressed in frame *i*
τ_L	Torque on end effector
$G(\theta)$	Gravity force matrix
H	Central angular momentum
${}^{i+1}\vec{k}_{zi}$	Unit vector along z axis
m_i	Mass of the ith link
${}^{i}\vec{M}_0^{i}$	Torque acting on the centre of the link expressed in frame *i*
MBD	Multibody dynamics
N	Number of links of an open chain manipulator
p^i	Position in the ith coordinate system
RP	Rapid Prototyping
T_e	External resultant torque
α_i	Offset/twist angle of link *I* (D-H)
${}^{i+1}\vec{\alpha}_{0i}$	Angular acceleration of ith coordinate in the *i*+1th coordinate system
θ_i	Joint angle of link *i*
τ_f	Friction Torque
τ_C	Coulomb friction torque
τ_{brk}	Breakaway friction torque
ω	Relative angular velocity
${}^{i+1}\vec{\omega}_{0i}$	Angular velocity of ith coordinate in the *i*+1th coordinate system
ω_{th}	Threshold velocity
${}^{i+1}\vec{v}_{0(i+1)}$	Translational velocity of ith coordinate in the *i*+1th coordinate system
v	Velocity/Relative velocity
v_R, v_c	Absolute velocities across terminals